JOURNAL OF THE KOREAN ASTRONOMICAL SOCIETY
38: 345 ~ 355, 2005

THE STAR CLUSTER SYSTEM OF THE MERGING GALAXY NGC 1487

HYE JIN LEE AND MYUNG GYOON LEE
Astronomy Program, SEES, Seoul National University, Seoul 151 - 742, Korea
E-mail: hyejin@astro.snu.ac.kr and mglee@astro.snu.ac.kr
(Received August 1, 2005; Accepted September 26, 2005)

ABSTRACT

We present a photometric study of the star cluster system in the merging galaxy NGC 1487, based on the BI photometry obtained from the F450W and F814W images in the HST/WFPC2 archive data. We have found about 560 star cluster candidates in NGC 1487, using the morphological parameters of the objects. We have investigated several photometric characteristics of the clusters: color-magnitude diagrams (CMDs), color distribution, spatial distribution, age, size and luminosity function. The CMD of the bright clusters with $18.5 < B < 24$ mag in NGC 1487 shows three major populations of clusters: a blue cluster population with $(B-I) \leq 0.45$, an intermediate-color cluster population with $0.45 < (B-I) \leq 1.55$, and a red cluster population with $(B-I) > 1.55$. The intermediate-color population is the most dominant among the three populations. The brightest clusters in the blue and intermediate-color populations are as bright as $B \approx 18$ mag ($M_B \approx -12$ mag), which are three magnitudes brighter than those in the red population. The blue and intermediate-color clusters are strongly concentrated on the bright condensations, while the red clusters are relatively more scattered over the galaxy. The CMD of these clusters is found to be remarkably similar to that of the clusters in the famous interacting system M51. From this we suggest that the intermediate-color clusters were, probably, formed during the merging process which occurred about 500 Myrs ago.

Key words : galaxy: individual — NGC 1487, merging galaxy, star cluster

I. INTRODUCTION

It is generally believed that the merging process of galaxies is one of the ways to form new stars and clusters. There are accumulating evidences based on the studies of merging and interacting galaxies, supporting this hypothesis (see references in Whitmore 2003). The best way to prove this hypothesis is to compare directly the cluster ages with the dynamical ages of the host galaxies. However, there are still only a handful number of merging galaxies of which star clusters were studied in detail, and it is not yet clearly known that star clusters were formed indeed during the merging process (e.g., Schweizer et al. 1996, Miller et al. 1997, Zepf et al. 1999, Keel & Bourne 2003). Recently Lee, Chandar & Whitmore (2005) found that the peak values in the age distribution of star clusters in the M51 system are consistent with the dynamical interaction time based on the models, concluding that those clusters were formed when the companion galaxy NGC 5195 was closest to NGC 5194. Therefore it is worthwhile to study star clusters in more merging and interacting galaxies to understand how star clusters are formed during the merging process.

In this paper we present a study of star clusters in NGC 1487, which is known as a merging galaxy. NGC 1487 is a peculiar late-type galaxy as shown in Fig. 1. The main body of this galaxy is characterized by three bright condensations in the central region and two long faint tidal tails extending in opposite direction out to 13 kpc, indicating that it is probably a merger (Agüero & Paolantonio 1997).

Basic information of NGC 1487 is listed in Table 1. We adopt a distance to this galaxy based on the radial velocity assuming the Hubble constant of $H_0 = 71$ km s^{-1} Mpc^{-1}, 10 Mpc. At the distance of 10 Mpc, one arcsecond in the sky corresponds to 48.55 pc. Absolute total magnitudes of NGC 1487 are similar to those of the Large Magellanic Cloud.

II. DATA REDUCTION

(a) HST Archive Data

We have used the F450W and F814W images of NGC 1487 in the HST archive, which are listed in Table 2. Field 1 is 41 arcsec north of Field 2. Fig. 2 displays a color map of Field 2, showing that bright condensations (APC1, APC2, APC3, and APC4) are well resolved into stars.

In Fig. 2 APC1 and APC3 are yellow to red, while APC2 and APC4 are much bluer and smaller than APC1 and APC3. This shows that stars were formed very recently in APC2 and APC4, while APC1 and APC3 show little evidence of recent star formation. This leads us to speculate that APC3 may be merging into APC1 and that APC2 and APC4 might have formed during the interaction of APC3 and APC1.

Corresponding Author: M. G. Lee

TABLE 1.
BASIC INFORMATION OF NGC 1487

Item	Value	Ref.[b]
RA (J2000)	$03^h55^m45.04^s$	1
Dec (J2000)	$-42°22'06.0''$	1
Morphological type	S pec (merger)	2
Total magnitude	$B^T = 12.33$, $M_B^T = -17.72$	3
	$V^T = 12.00$, $M_V^T = -18.04$	3
Radial velocity	$v_h = 857 \pm 15$ km s^{-1}	3
Systemic velocity	$v_{GSR} = 711 \pm 15$ km s^{-1}	3
Distance	10.0±0.2 Mpc[a]	3
Foreground reddening	$E(B-I) = 0.028$	4

[a] For $H_0 = 71$ km s^{-1} Mpc^{-1}
[b] References:
1. RC3 (de Vaucouleurs et al. 1991);
2. Sandage & Tammann (1981);
3. Agüero et al. (1997);
4. Schlegel et al. (1998).

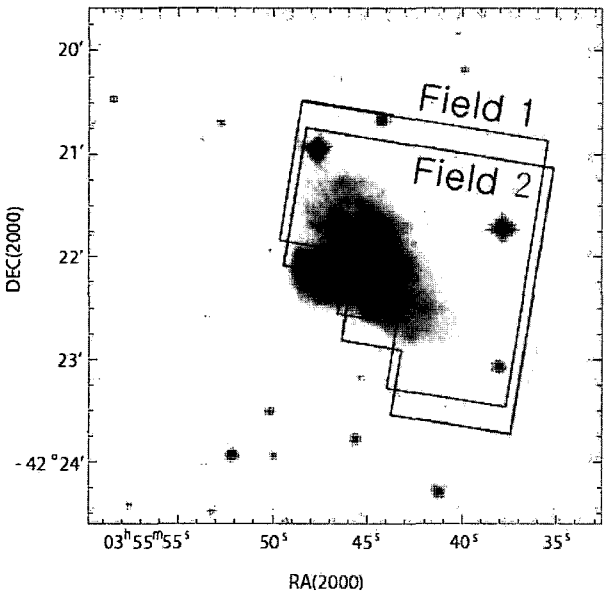

Fig. 1.— A Palomar Digitized Sky Survey image of NGC 1487 showing positions of the HST/WFPC2 fields of NGC 1487 (labelled as Field 1 and Field 2, respectively)

(b) Photometry

We have derived the magnitudes of the objects in the WFPC2 images using HSTPHOT which is designed for the photometry of HST/WFPC2 images (Dolphin 2000a, 2000b, 2003). Instrumental magnitudes were obtained using the aperture photometry with aperture radii of 2.1 pixels and 1.4 pixels for PC and WF chips, respectively. We have estimated the aperture correction using the bright clusters, deriving $\Delta(B) = -0.637 \pm 0.009$ for the PC chip (aperture radii of 8 pixels) and -0.700 ± 0.009 the WF chips (aperture radii of 5 pixels). We applied the aperture correction only for the B magnitudes, keeping the $(B-I)$ color provided by the HSTPHOT. Instrumental magnitudes were converted onto the standard BI system using the calibration given in Holtzman et al. (1995) and Jordan et al. (2004) as below:

TABLE 2.
HST ARCHIVE DATA FOR NGC 1487

	Field 1	Field 2
R.A.(J2000)	$03^h55^m44.94^s$	$03^h55^m44.94^s$
Dec. (J2000)	$-42°21'54.44''$	$-42°21'13.44''$
Filter	F450W(900s×2)	F450W(900s×2)
	F814W(800s×2)	F814W(800s×2)
Observation Date	April 3 1995	
Program ID and PI	GO−5396 and Stephan Zepf	

if $(B-I)_{1.3} < 0$,

$$\begin{cases} I = m_{F814W} - 0.025(B-I)_{1.3} - 0.009(B-I)_{1.3}^2 - 0.021 \\ B = m_{F450W} + 0.087(B-I)_{1.3} - 0.008(B-I)_{1.3}^2 + 0.126 \end{cases} \quad (1)$$

if $(B-I)_{1.3} > 0$,

$$\begin{cases} I = m_{F814W} - 0.012(B-I)_{1.3} - 0.003(B-I)_{1.3}^2 - 0.021 \\ B = m_{F450W} + 0.193(B-I)_{1.3} - 0.047(B-I)_{1.3}^2 + 0.126 \end{cases} \quad (2)$$

where m_{F450W} and m_{F814W} are WFPC2 flight system magnitude, and $(B-I)_{1.3} \equiv (B-I) - 1.3$.

We have done artificial star tests using the HSTPHOT to estimate the completeness of our photome-

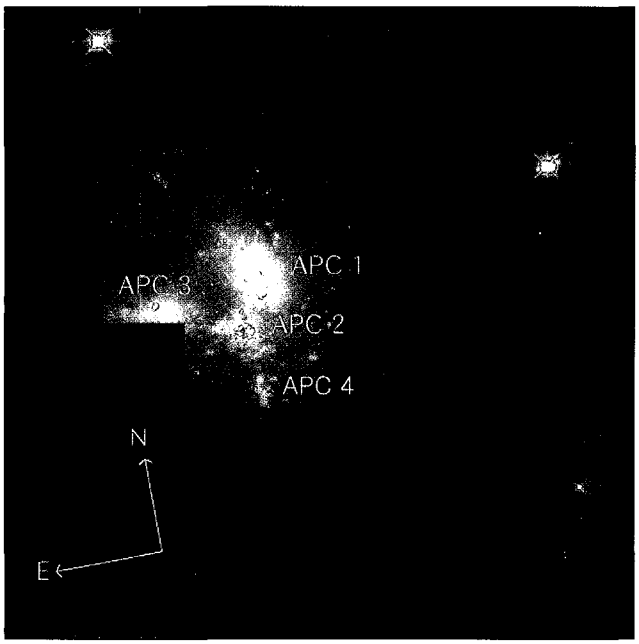

Fig. 2.— A color map of the HST/WFPC2 image of NGC 1487–Field 2. Orientation is marked by the arrows. Bright condensations are labelled as APC1, APC2, APC3 and APC4 (Agüero & Paolantonio 1997).

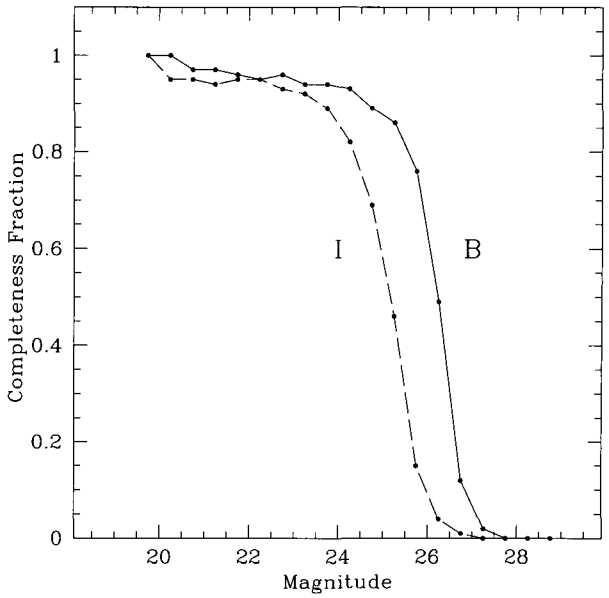

Fig. 3.— Completeness fraction vs. B magnitude (solid line) and I(dashed line) magnitude for artificial stars.

try. These experiments were carried out on the Fields 1 and 2, respectively. We added artificial stars in each image, and counted the number of recovered stars using the same procedure to estimate the completeness. Fig. 3 displays the completeness vs. B and I magnitudes. The 50 per cent of completeness limit is estimated to be $B \approx 26.2$ mag and $I \approx 25.2$ mag. Since clusters are more extended than stars, completeness of the clusters at given magnitude may be slightly lower than that of the stars.

(c) Cluster Selection

We have selected star cluster candidates following the method described in Dolphin & Kennicutt (2002a, 2002b). Dolphin & Kennicutt (2002a) suggested that the sharpness provided by the HSTPHOT can be used efficiently and reliably to select cluster candidates in the WFPC2 images of galaxies at the distance of 10–30 Mpc. They applied the sharpness method to find the clusters in the HST/WFPC2 images of NGC 3627 the distance to which is very similar to that to NGC 1487. Sharpness of the HSTPHOT is defined to be zero for point sources in the images, and is expected to be smaller than zero for extended sources such as clusters and galaxies.

We have used artificial stars in the I-band images to check the distribution of sharpness of point sources as a function of magnitude. It is found that the sharpness of the artificial stars is on average zero, with a scatter increasing with the increasing magnitude. We have derived the following equations for the $\pm 2.5\sigma$ envelopes in the diagram of the sharpness values vs. I magnitudes of artificial stars:

$$Field\ 1 \begin{cases} PC\ sharpness = -0.314\, e^{0.594(I-26)} \\ WF2\ sharpness = -0.518\, e^{0.559(I-26)} \\ WF3\ sharpness = -0.129\, e^{0.397(I-26)} \\ WF4\ sharpness = -0.171\, e^{0.445(I-26)} \end{cases} \quad (3)$$

$$Field\ 2 \begin{cases} PC\ sharpness = -0.236\, e^{0.513(I-26)} \\ WF2\ sharpness = -0.153\, e^{0.533(I-26)} \\ WF3\ sharpness = -0.158\, e^{0.472(I-26)} \\ WF4\ sharpness = -0.236\, e^{0.481(I-26)} \end{cases} \quad (4)$$

Fig. 4 displays the sharpness vs. I magnitudes for the detected sources in Fields 1 and 2. It is seen in Fig. 4 that most of the sources are located between the upper and lower envelopes. These are point sources, mostly stars and some unresolved clusters. In addition, a significant number of sources are found to be located below the -2.5σ envelopes. These sources are slightly extended sources and we consider them to be star cluster candidates. The crosses represent the sources classified as extended sources by the HSTPHOT, which are mostly background galaxies. The total number of star cluster candidates found this way in Field 1 and Field 2 is about 560. We have also inspected the stellarity of these objects obtained using the Source EXtractor (Bertin & Arnouts 1996), and have found that the stellarities of these cluster candidates are mostly smaller than 0.2, confirming that these cluster candidates are indeed larger than point sources (stars). From now on we call the cluster candidates as clusters, and the point

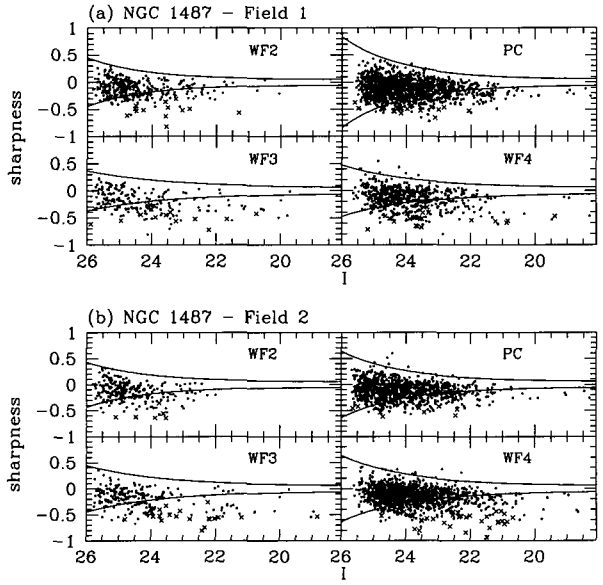

Fig. 4.— Sharpness value vs. I magnitude of detected sources Field 1 and Field 2 of NGC 1487. The curved lines represent the envelopes of width = ± 0.05 and $\sigma = \pm 2.5$. The crosses denote sources which were classified as extended objects (mostly galaxies) in the HSTPHOT.

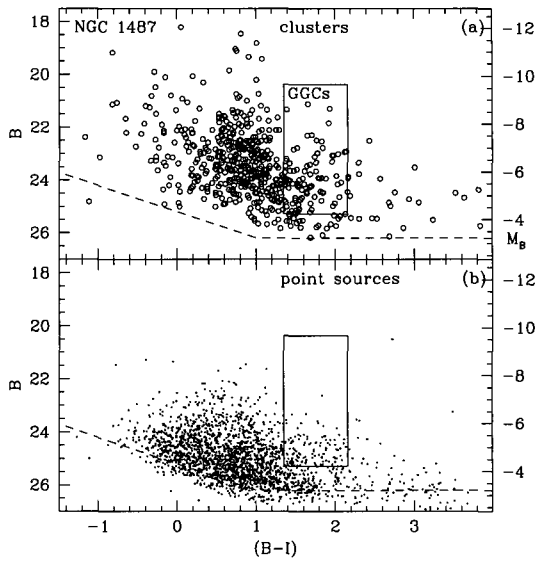

Fig. 5.— (a) CMD of clusters in NGC 1487. The rectangular box denotes the region where globular clusters of our Galaxy would occupy when they are placed at the distance of NGC 1487 with foreground reddening correction. (b) CMD of point sources which are mostly stars and some unresolved clusters. The dashed lines represent the isolimiting magnitude lines for 50 % completeness of B-band photometry.

sources as stars. Table 3 lists a sample of 60 bright clusters with $B < 22$ mag in NGC 1487. The catalog of the entire clusters can be obtained from the authors.

III. RESULTS

(a) Color Magnitude Diagram

Fig. 5 shows color-magnitude diagram (CMD) for cluster candidates and point sources (mostly stars) we found in NGC 1487. Several features are noted in Fig. 5: (1) The range of the cluster color is large from $(B-I) \approx -1$ to 2.5 for $B < 24$ mag; (2) Most of the clusters in NGC 1487 are bluer than the Galactic globular clusters (Harris 1996); (3) The brightest clusters in NGC 1487 ($M_B \approx -12$) are brighter than the brightest Galactic globular clusters; (4) The lack of faint blue clusters is due to the incompleteness of our data, as shown by the limiting magnitude line; (5) The stars seen in Fig. 5 (b) are mostly young massive stars (blue main-sequence stars, supergiants and giants).

(b) Color Distribution

We have derived the color distribution of bright stars and clusters with $B < 24$ mag, as plotted in Fig. 5. We used only the bright objects to reduce the effect of incompleteness due to photometry limit and any contamination due to background galaxies.

It is found in Fig. 6 that the color distribution of the clusters shows a strong peak at $(B-I) \approx 0.8$, and two weaker peaks at $(B-I) \approx 0.2$ and 1.8, respectively. Thus the cluster system of NGC 1487 can be divided into three populations: blue population ($(B-I) \leq 0.45$), intermediate-color population ($0.45 < (B-I) \leq 1.55$) and red population ($(B-I) > 1.55$). The intermediate-color population is the most dominant among these. Most of the red population have colors bluer than the red boundary of the Galactic globular clusters, but some of them have colors redder than this boundary and get fainter as the colors get redder. Therefore, the red population may be composed of mostly old globular clusters. Some of them may be younger clusters highly reddened by the internal dust in NGC 1487. However, it is not possible to separate them from BI photometry only.

In contrast, Fig. 6 illustrates that the color distribution of the bright stars with $B < 24$ mag (dashed line) shows only a single broad peak, which is 0.4 bluer than that of the intermediate-color clusters. This indicates that the formation history of stars may be different from that of clusters in NGC 1487.

(c) Spatial Distribution

We have investigated the spatial distribution of the bright clusters with $B < 24$ mag in Fig. 7, and point sources with $B < 26.2$ mag, 50% completeness level, in

TABLE 3.
CLUSTER CANDIDATES WITH $B < 22$ IN NGC 1487

ID	RA(^{h} ^{m} ^{s})(J2000)	DEC($^\circ$ $'$ $''$)(J2000)	B	B–I	r_c[arcsec]
4	3 55 45.18	-42 22 13.7	19.427 ± 0.000	1.076 ± 0.000	0.395 ± 0.000
13	3 55 45.23	-42 22 14.2	21.684 ± 0.032	1.037 ± 0.032	0.464 ± 0.000
14	3 55 45.32	-42 22 14.2	19.120 ± 0.000	0.755 ± 0.000	0.596 ± 0.000
19	3 55 45.35	-42 22 14.4	19.861 ± 0.000	0.662 ± 0.000	0.899 ± 0.000
20	3 55 45.46	-42 22 14.4	21.586 ± 0.032	0.847 ± 0.045	0.848 ± 0.000
22	3 55 45.11	-42 22 15.2	21.511 ± 0.000	0.924 ± 0.000	0.492 ± 0.000
24	3 55 45.21	-42 22 15.1	18.465 ± 0.000	0.812 ± 0.000	0.874 ± 0.000
29	3 55 45.37	-42 22 15.3	20.801 ± 0.000	-0.075 ± 0.000	0.777 ± 0.000
30	3 55 45.09	-42 22 16.0	18.825 ± 0.000	1.010 ± 0.000	0.274 ± 0.000
31	3 55 45.44	-42 22 15.3	21.864 ± 0.032	-0.415 ± 0.055	1.318 ± 0.032
35	3 55 45.10	-42 22 16.2	20.902 ± 0.000	0.769 ± 0.000	0.976 ± 0.000
43	3 55 45.17	-42 22 17.0	20.745 ± 0.000	1.033 ± 0.000	0.506 ± 0.000
44	3 55 45.50	-42 22 16.4	21.608 ± 0.000	0.606 ± 0.032	1.424 ± 0.000
45	3 55 44.99	-42 22 17.7	20.846 ± 0.000	0.791 ± 0.000	0.188 ± 0.000
51	3 55 45.64	-42 22 19.1	21.464 ± 0.000	0.810 ± 0.000	1.380 ± 0.000
52	3 55 44.81	-42 22 20.8	21.248 ± 0.000	-0.346 ± 0.000	1.864 ± 0.032
54	3 55 46.14	-42 22 18.9	21.123 ± 0.032	1.657 ± 0.032	0.936 ± 0.000
56	3 55 45.36	-42 22 21.1	21.624 ± 0.000	0.531 ± 0.032	0.819 ± 0.000
66	3 55 45.39	-42 21 53.6	21.458 ± 0.158	0.709 ± 0.224	0.945 ± 0.130
68	3 55 45.01	-42 21 54.6	21.424 ± 0.152	0.772 ± 0.214	1.144 ± 0.141
74	3 55 44.35	-42 22 2.0	21.680 ± 0.045	0.564 ± 0.063	1.747 ± 0.179
75	3 55 44.73	-42 22 1.4	21.873 ± 0.155	0.936 ± 0.212	0.715 ± 0.148
76	3 55 44.95	-42 22 1.1	20.477 ± 0.126	-0.273 ± 0.210	0.799 ± 0.134
78	3 55 45.06	-42 22 2.6	21.903 ± 0.152	0.673 ± 0.279	1.018 ± 0.152
80	3 55 44.61	-42 22 3.8	20.212 ± 0.122	1.005 ± 0.158	0.927 ± 0.100
81	3 55 44.82	-42 22 3.7	21.957 ± 0.214	0.816 ± 0.290	1.236 ± 0.187
84	3 55 44.70	-42 22 5.3	20.302 ± 0.089	0.333 ± 0.141	0.236 ± 0.089
86	3 55 44.87	-42 22 5.4	20.106 ± 0.089	-0.148 ± 0.152	0.519 ± 0.095
87	3 55 44.84	-42 22 6.2	20.929 ± 0.145	0.066 ± 0.200	0.605 ± 0.130
89	3 55 44.67	-42 22 7.2	21.139 ± 0.045	-0.818 ± 0.071	1.784 ± 0.243
90	3 55 44.78	-42 22 7.2	21.489 ± 0.164	-0.266 ± 0.253	0.598 ± 0.173
94	3 55 44.92	-42 22 8.1	21.863 ± 0.184	0.883 ± 0.243	0.857 ± 0.152
100	3 55 45.24	-42 22 10.0	21.331 ± 0.145	1.389 ± 0.176	0.420 ± 0.100
101	3 55 45.47	-42 22 9.9	21.352 ± 0.152	0.701 ± 0.230	0.784 ± 0.122
104	3 55 45.21	-42 22 11.0	20.754 ± 0.126	0.751 ± 0.161	0.263 ± 0.089
135	3 55 42.51	-42 21 53.8	21.300 ± 0.000	1.934 ± 0.000	1.092 ± 0.000
149	3 55 44.28	-42 21 50.2	21.072 ± 0.032	-0.761 ± 0.045	2.059 ± 0.000
150	3 55 44.15	-42 21 41.3	21.899 ± 0.000	-0.192 ± 0.032	1.890 ± 0.032
151	3 55 44.33	-42 21 49.7	21.299 ± 0.000	0.283 ± 0.032	2.774 ± 0.000
157	3 55 44.36	-42 21 36.2	19.352 ± 0.000	0.909 ± 0.000	0.546 ± 0.000
171	3 55 45.37	-42 21 52.0	19.045 ± 0.000	0.742 ± 0.000	0.739 ± 0.000
153	3 55 44.73	-42 22 4.9	20.070 ± 0.009	0.198 ± 0.014	0.590 ± 0.012
154	3 55 45.26	-42 22 10.5	21.197 ± 0.034	1.062 ± 0.040	0.830 ± 0.015
155	3 55 44.64	-42 22 2.4	21.007 ± 0.025	0.885 ± 0.033	1.241 ± 0.018
156	3 55 45.85	-42 22 11.8	21.347 ± 0.027	1.138 ± 0.034	0.411 ± 0.019
157	3 55 44.97	-42 22 0.4	20.813 ± 0.027	-0.323 ± 0.042	0.726 ± 0.016
158	3 55 46.84	-42 22 13.3	21.497 ± 0.021	0.532 ± 0.044	0.806 ± 0.022
159	3 55 44.81	-42 22 4.9	21.641 ± 0.024	0.744 ± 0.034	0.912 ± 0.037
161	3 55 46.69	-42 22 9.7	21.980 ± 0.030	0.896 ± 0.036	0.426 ± 0.016
163	3 55 46.53	-42 22 11.0	21.987 ± 0.032	0.729 ± 0.043	0.872 ± 0.033
236	3 55 43.19	-42 22 0.9	21.879 ± 0.033	0.783 ± 0.039	1.373 ± 0.020
333	3 55 45.21	-42 22 15.7	21.359 ± 0.016	0.952 ± 0.023	0.267 ± 0.011
336	3 55 45.09	-42 22 27.8	21.658 ± 0.018	0.569 ± 0.025	2.014 ± 0.048
337	3 55 45.39	-42 22 15.5	21.815 ± 0.048	0.533 ± 0.055	1.217 ± 0.024
338	3 55 45.09	-42 22 34.2	21.707 ± 0.035	0.881 ± 0.064	0.459 ± 0.020
342	3 55 45.10	-42 22 32.7	21.766 ± 0.041	0.227 ± 0.062	0.382 ± 0.018
345	3 55 45.01	-42 22 30.9	21.974 ± 0.040	0.025 ± 0.083	0.991 ± 0.031
435	3 55 47.16	-42 22 5.4	19.904 ± 0.008	-0.285 ± 0.015	3.344 ± 0.019
436	3 55 47.20	-42 22 5.5	19.176 ± 0.008	-0.814 ± 0.016	2.059 ± 0.015

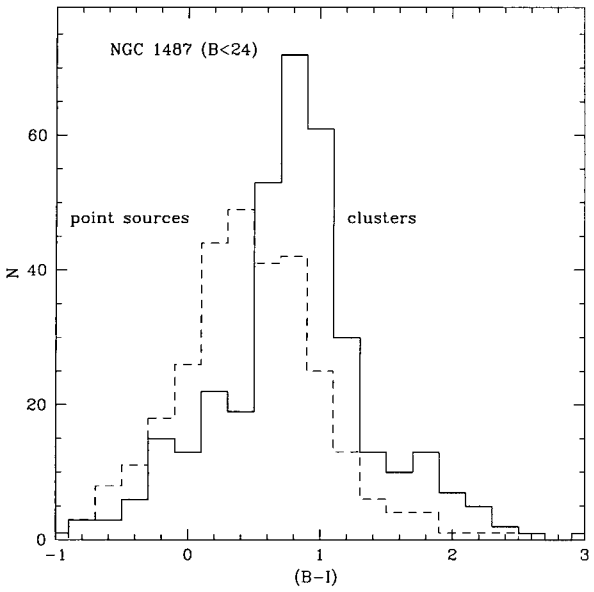

Fig. 6.— Color distribution of the bright clusters (solid line) and point sources (dashed line) with $B < 24$ mag (mostly stars) in NGC 1487.

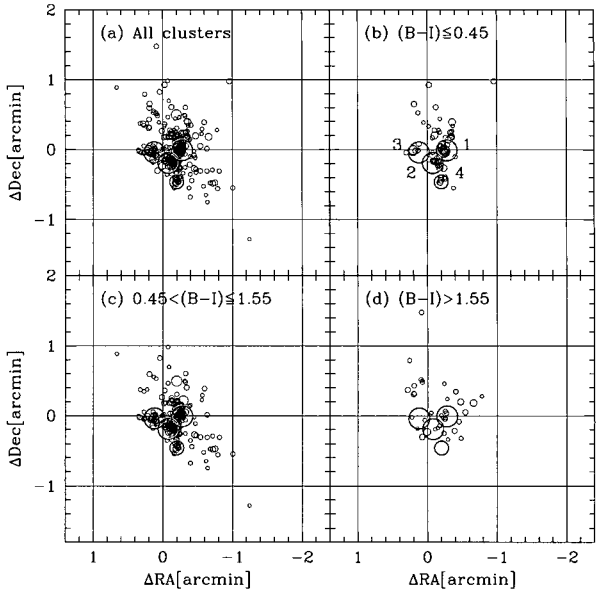

Fig. 7.— Spatial distribution of clusters with $B < 24$ mag in NGC 1487. (a) all clusters, (b) the blue cluster population ($(B-I) \leq 0.45$), (c) the intermediate-color cluster population ($0.45 < (B-I) \leq 1.55$), and (d) the red cluster population ($(B-I) > 1.55$). The size of the symbols represents the relative magnitude (the larger the symbols are, the brighter the clusters are). Large circles represent the positions of the bright condensations APC1, APC2, APC3, and APC4).

Fig. 8. Although point sources have only one broad peak in the color distribution, we have adopted the same color boundaries as for clusters to compare their spatial distribution. These figures show the following features: (1) Blue and intermediate-color clusters are strongly concentrated around the three bright condensations (APC1, APC2, and APC3), while red clusters are rather scattered over the region; (2) The pattern for stars is similar to that for clusters in general; (3) However, the stars show a new feature, a narrow concentration of stars located at ΔRA$\approx$ 0.4 arcmin and ΔDec $\approx$ 1.2 arcmin in the NE direction. This region is mostly composed of blue and intermediate-color stars.

Figs. 9 and 10 display, respectively, the CMDs of the clusters and the stars in the bright condensations, APC1, APC2, APC3 and APC4. Several features are noted in these figures: (1) The main population of the condensations is intermediate-color clusters; (2) However, there are significant differences among the condensations. While APC1 contains 17 bright blue clusters with $(B-I) \approx 0.0$, the other condensations include few such clusters. The brightest cluster in APC1 with $B = 18.215 \pm 0.006$ mag is the brightest in the entire sample of clusters, and has an absolute magnitude of $M_B = -11.8$ mag. It is very blue with $(B-I) = 0.054 \pm 0.009$; (3) APC2 includes several intermediate-color clusters much brighter than those in other condensations; (4) APC3 and APC4 contain mostly intermediate-color clusters which are fainter than $B \approx 22$ mag; (5) These trends for the clusters are also seen in the CMDs of the stars, but much less obviously (probably due to severe crowding).

(d) Cluster Size

We have estimated the core radii r_c of the clusters using the HSTPHOT. *Calcclus* routine in the HSTPHOT provides information of physical properties of slightly extended objects like the star clusters we found in NGC 1487. The half light radii r_h can be roughly estimated from the core radii using the equation

$$r_h = r_c\sqrt{(2^{(1/0.26)} - 1)/0.73} = 4.28 r_c \qquad (5)$$

which was derived using equation (10) in Dolphin & Kennicutt (2002a)

$$L(< r) = L[1 - (1 + 0.73\frac{r^2}{r_c^2})^{-0.26}] \qquad (6)$$

HSTPHOT does not provide reliable PSF-fitting photometry for objects with core radii larger than one pixel (corresponding 4.7 pc) (Dolphin & Kennicutt 2002b) so that we used only clusters with core radii smaller than 5 pc and $B < 24$ mag. In Fig. 11 we display the core radii versus B magnitude diagram for the 239 clusters with $B < 24$ mag. In Fig. 11 the lower envelope starts

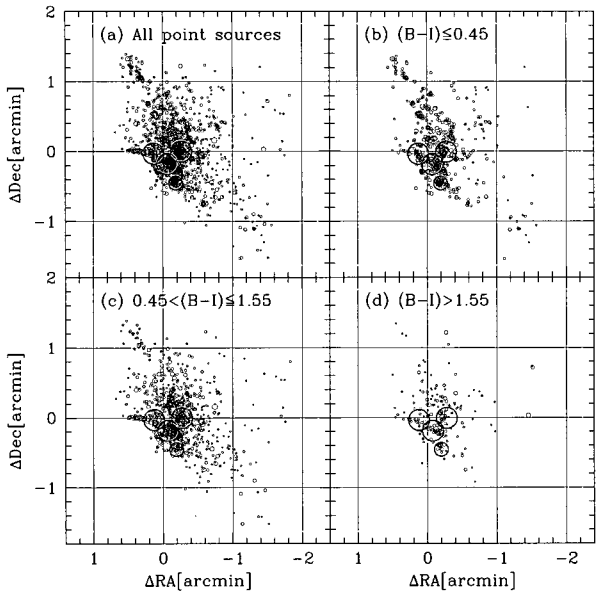

Fig. 8.— Same as Fig. 7, but for the point sources with $B < 26.2$ mag.

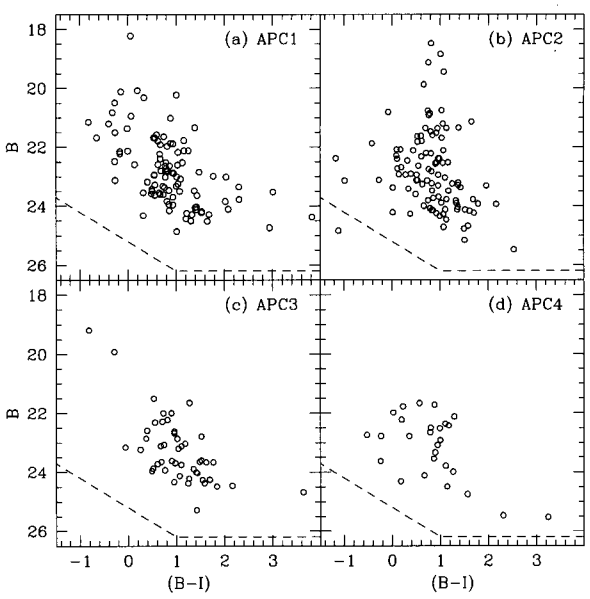

Fig. 9.— CMDs of the clusters in the bright condensations (APC1, APC2, APC3 and APC4).The dashed lines represent the iso-limiting magnitude lines for 50 % completeness of B-band photometry for star.

increasing at $B > 23$ mag, which is due to the fact the fraction of small faint clusters missing is increasing as the magnitude increases. Fig. 11 shows that the upper envelope of the core radii increases roughly with magnitudes. Further studies are needed to understand the cause for this.

Fig. 12 illustrates the distribution of the core radii of the clusters with $B < 24$ mag. It is found: (1) that the core radii range from 0.5 pc to 4.7 pc, with a peak at $r_c \approx 1.0$ pc and the mean value of $r_c = 1.3 \pm 0.8$ for 239 clusters; (2) the blue clusters show almost flat distribution, while the intermediate-color and red clusters show peaks at $r_c \approx 1.5$ and 1.0 pc, respectively; (3) The mean values of the core radii are $r_c = 1.7 \pm 1.1$ for the 60 blue clusters, $r_c = 1.2 \pm 0.6$ for 160 intermediate-color clusters, and $r_c = 1.2 \pm 0.7$ the 19 red clusters. Thus the core radii of the blue clusters are on average larger than those of intermediate-color and red clusters.

(e) Cluster Age and Mass

It is not possible to measure age and mass of the clusters reliably from BI photometry. However, we can estimate roughly the range of cluster age and mass using the population synthesis models. In Fig. 13 we compared the NGC 1487 clusters with the GALAXEV stellar population synthesis models provided by Bruzual & Charlot (2003) on the CMD . The synthesis models are based on the stellar evolutionary tracks for the metallicity $Z = 0.008$ of the Padova group which is similar to the mean metallicity of LMC, $[F/H] \approx -0.3$ (Luck et al. 1998), adopting the Salpeter stellar initial mass function (with power index $x = 1.35$) and the stellar mass range of 0.1 to 100 $M_\odot$. Fig. 12 shows that the mass of the clusters ranges from $10^2 M_\odot$ to $10^6 M_\odot$ and the age of the clusters ranges from a few Myrs to the age of the old globular clusters. The peaks seen in the color distribution of the clusters, $(B - I) = 0.2$ and 0.8, correspond to the ages 15 Myrs and 500 Myrs, respectively. Therefore, the most dominant bright cluster population in NGC 1487 appears to have formed about 500 Myrs ago.

(f) Luminosity Function

We have derived the B-band luminosity function of the clusters in NGC 1487. We applied the completeness correction derived from artificial star experiment to the cluster luminosity function, so that the resulting luminosity functions must be flatter at the faint end than the intrinsic luminosity functions. The completeness of our photometry we estimated using artificial stars cannot be directly applied to the sample of clusters, because the detection of the clusters depends not only on the completeness of the photometry but also on the cutoff envelope shown in Fig. 4. Therefore, we consider the luminosity function of the clusters to be reliable for the range $B < 24$ mag. We consider that the contamination due to foreground stars is negligible in deriving the luminosity function of the clusters in NGC 1487. Fig. 14 displays the luminosity function of the clusters thus derived: (a) the blue clusters with $(B - I) \leq 0.45$, (b) the blue clusters

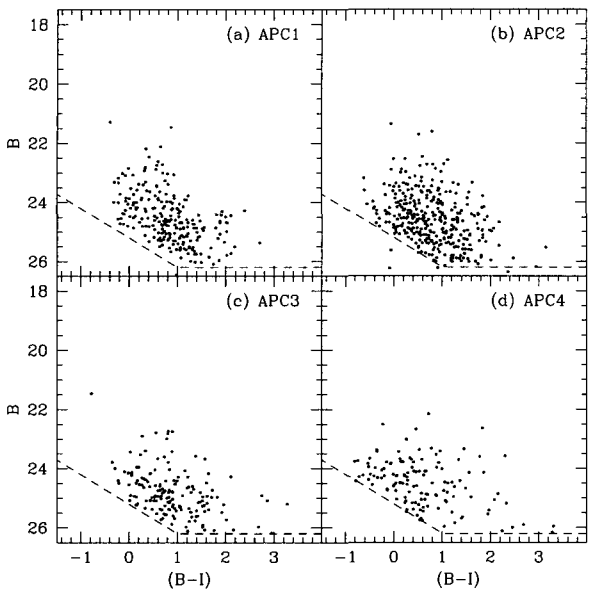

Fig. 10.— CMDs of the stars in the bright condensations (APC1, APC2, APC3 and APC4). The dashed lines represent the iso-limiting magnitude lines for 50 % completeness of B-band photometry for stars.

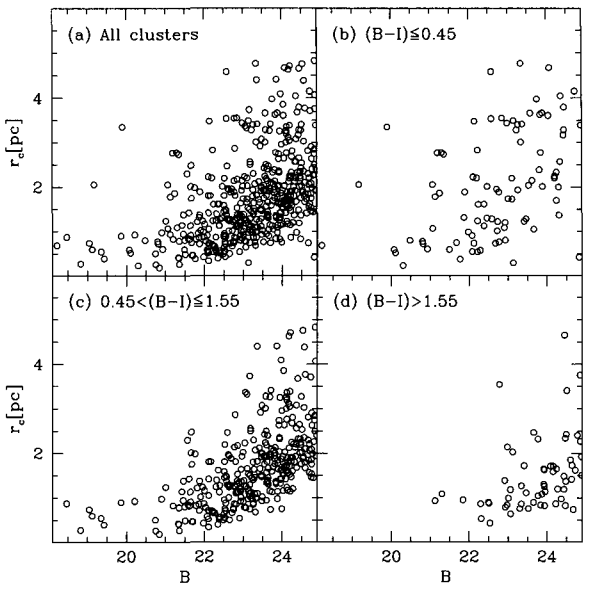

Fig. 11.— Core radii vs. B magnitude diagrams for the cluster population: (a) all clusters, (b) blue clusters, (c) intermediate-color clusters, and (d) red clusters.

with $(B-I) \leq 0.8$, (c) the intermediate-color clusters with $0.45 < (B-I) \leq 1.55$, (d) the red clusters with $(B-I) > 1.55$, and (e) all clusters. It is seen in Fig. 14 that the luminosity functions of the clusters with $B < 24$ mag follow approximately a power-law. We have fitted the bright part of uncorrected luminosity function with the power law, obtaining the logarithmic slopes. These values are listed in Table 4.

The luminosity function of the globular clusters in our Galaxy shows a Gaussian form with a peak at $M_B \approx -6.6$ mag. It is intriguing that even the luminosity function of the red clusters in NGC 1487 does not show a Gaussian form with a peak at $M_B \approx -6.6$ mag.

IV. DISCUSSION

We have compared the properties of the cluster system in NGC 1487 with those of the cluster systems in other galaxies. We have found that the peak values of the core radii of the clusters in NGC 1487 are about 1.5 pc and 1 pc for intermediate-color clusters and red clusters, respectively. For comparison, Dolphin & Kennicutt (2002b) found, using the same HST-PHOT, that the core radii distribution of the young clusters in an interacting galaxy NGC 3627 is centered at $r_c = 1.53 \pm 0.15$ with a half-width at half-maximum (HWHM) of 0.88 pc. Thus the core radii of the young clusters in NGC 1487 and NGC 3627 are very similar. On the other hand, Seth et al. (2004) derived a mean core radius, 2.5 pc, for 12 globular clusters in the LMC using data from Mackey & Gilmore (2003), and the mean core radius of Galactic globular clusters with $M_V < -6.5$ mag is found to be 1.5 pc (Harris 1996). Therefore the mean core radius of the red clusters in NGC 1487 is smaller than those of the globular clus-

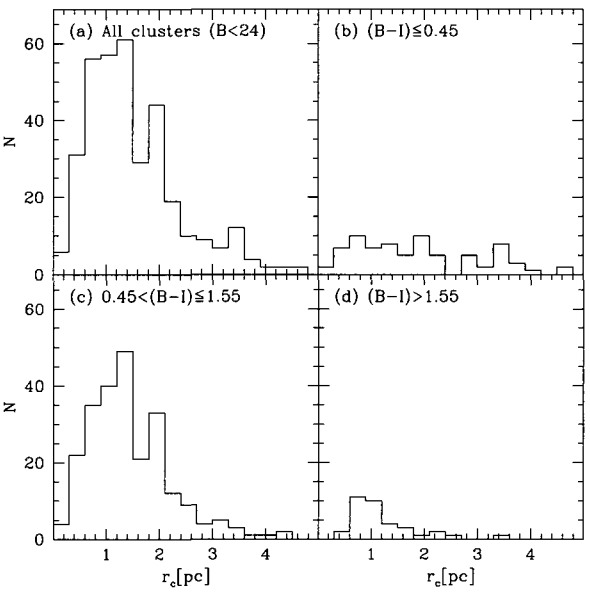

Fig. 12.— The distribution of the core radii of the bright clusters with $B < 24$ mag.

TABLE 4.
LOGARITHMIC SLOPES OF THE B-BAND LUMINOSITY FUNCTIONS OF THE CLUSTERS IN NGC1487

cluster population	B	$-d\log N/dB$	M_B	$d\log N/d\log L_B$
$(B-I) \leq 0.45$	$20.0 < B < 23.5$	0.25 ± 0.06	$-10.0 < M_B < -6.5$	-0.61 ± 0.15
$(B-I) \leq 0.8$	$19.0 < B < 23.5$	0.38 ± 0.03	$-11.0 < M_B < -6.5$	-0.96 ± 0.08
$0.45 < (B-I) \leq 1.55$	$20.5 < B < 23.5$	0.45 ± 0.06	$-9.5 < M_B < -6.5$	-1.13 ± 0.15
$(B-I) > 1.55$	$21.0 < B < 23.5$	0.44 ± 0.14	$-9.0 < M_B < -6.5$	-1.09 ± 0.35
all clusters	$20.0 < B < 23.5$	0.43 ± 0.04	$-10.0 < M_B < -6.5$	-1.08 ± 0.10

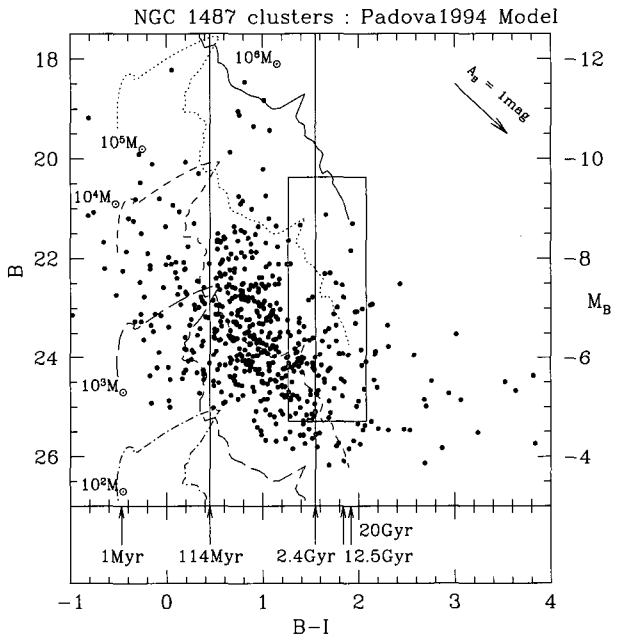

Fig. 13.— Comparison of NGC 1487 clusters with stellar population synthesis models (Bruzual & Charlot 2003) on the CMD. The curved lines represent simple stellar population models for $10^6 M_\odot$ (solid line), $10^5 M_\odot$(dot line), $10^4 M_\odot$ (short-dashed line), $10^3 M_\odot$ (long-dashed line), and $10^2 M_\odot$ (dot-long-dashed line), shifted according to the distance and foreground reddening of NGC 1487. The models are based on the stellar evolutionary tracks for the metallicity $z = 0.008$ of the Padova group, adopting the Salpeter stellar initial mass function. Three vertical lines are boundary lines separating cluster populations. The age below boundary line denotes the upper limit for each population. The rectangular box denotes the region for the Galactic globular clusters. The arrow indicates reddening direction for $A_B = 1$ mag.

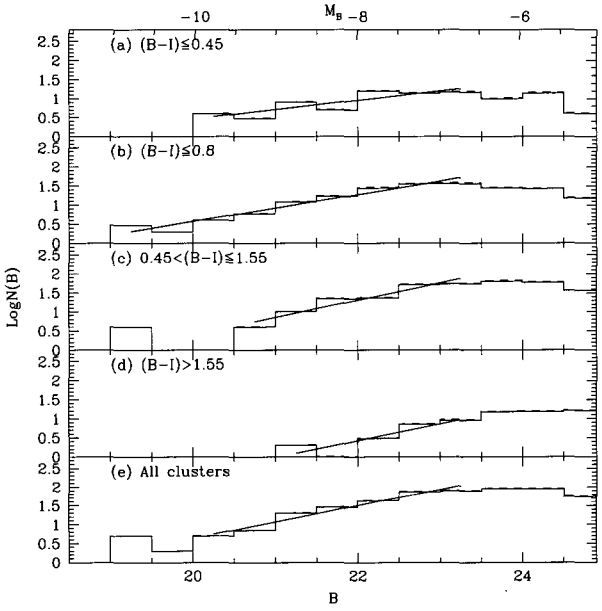

Fig. 14.— Luminosity functions for the cluster populations in NGC 1487. The solid histograms denote the observed luminosity functions, while the dashed histograms represent the luminosity functions corrected for completeness of stellar photometry. Linear lines are power-law fits to the completeness-corrected luminosity functions.

ters in the LMC and our Galaxy. Explanation of this difference needs further studies.

The luminosity functions of the bright young clusters in NGC 1487 are found to be fitted by the power law with logarithmic slopes. The derived slopes range from $d\log N/d\log L_B = -1.08 \pm 0.10$ for all clusters and -0.96 ± 0.08 for blue clusters with $(B-I) < 0.8$. For comparison, Dolphin & Kennicutt (2002a) obtained, using the same method as we used here, the luminosity function of the clusters in NGC 3627, and derived the values for the slopes of $d\log N/d\log L_V = -1.43 \pm 0.12$ for all clusters with $M_V < -8$ mag and -1.22 ± 0.23 for blue clusters with $(V-I) < 0.5$. Therefore, the luminosity functions of clusters in NGC 1487 are slightly flatter than those for NGC 3627.

We have compared the clusters in NGC 1487 with

those in M51 in the CMD in Fig. 15. M51 is a famous interaction system of two galaxies (NGC 5194 and NGC 5195). Lee, Chandar, & Whitmore (2005) presented HST/WFPC2 *UBVI* photometry of about 400 clusters in M51, and derived several physical parameters including age and size. They found evidence that the intermediate-color clusters in M51 were mostly formed when the companion galaxy (NGC 5195) passed the host galaxy (NGC 5194). The crossing time of NGC 5195 depends on the dynamical models, but is in the range of a few hundred Myrs ago. Fig. 14 shows that the NGC 1487 clusters are remarkably similar to M51 clusters. This lead us to suggest that most star clusters in NGC 1487 were probably formed during the merging process about 500 Myrs ago. APC3 may be a companion system merging onto the main body of NGC 1487, as described in Section 1. It will be interesting to investigate this conclusion using the dynamical modelling of NGC 1487.

V. SUMMARY

We present a photometric study of the star cluster system in the merging galaxy NGC 1487, based on the *BI* photometry obtained from the F450W and F814W images in the HST/WFPC2 archive data.

1. We have found about 560 star cluster candidates in NGC 1487, using the morphological parameters of the objects detected in the images.

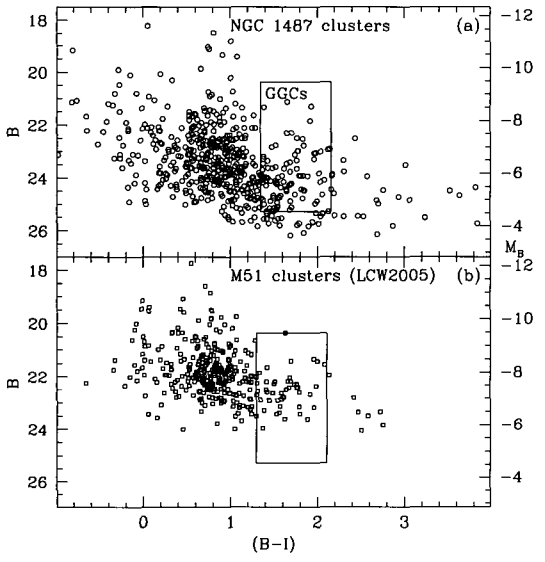

Fig. 15.— Comparison of star clusters in NGC 1487 (this study) and M51 (Lee, Chandar & Whitmore 2005) in the CMD. The magnitudes and colors of M51 clusters were shifted according to the distance and foreground reddening of NGC 1487. Note the similarity between the two galaxies.

2. The CMD and color distribution of the bright clusters show that the cluster system of NGC 1487 is composed mainly of three populations: a blue cluster population with $(B-I) \leq 0.45$, an intermediate-color cluster population with $0.45 < (B-I) \leq 1.55$, and a red cluster population with $(B-I) > 1.55$. The intermediate-color population is the most dominant among the three populations. The brightest clusters in the blue and intermediate-color populations are as bright as $B \approx 18$ mag ($M_B \approx -12$ mag), which are three magnitudes brighter than those in the red population.
3. The blue and intermediate-color clusters are strongly concentrated on the bright condensations, while the red clusters are more scattered over the galaxy.
4. The luminosity functions of the blue and intermediate color clusters are approximately fitted by the power-law.
5. The CMD of these clusters is found to be very similar to that of the clusters in M51. From this we suggest that the intermediate-color clusters were, probably, formed during the merging process which occurred about 500 Myrs ago.

ACKNOWLEDGEMENTS

We are grateful to Sang Chul Kim and Andrew E. Dolphin who provided helpful advices for using the HSTPHOT, and to the anonymous referee for very useful comments which improved the original manuscript of this paper. This is in part supported by the ABRL(R14-2002-058-010000-0).

REFERENCES

Agüero, E. L., & Paolantonio S., 1997, The Peculiar Galaxy NGC 1487, AJ, 114, 102

Bertin, E., & Arnouts, S., 1996, SExtractor: Software for source extraction, A&AS, 117, 393

Bruzual, G., & Charlot, S., 2003, Stellar population synthesis at the resolution of 2003, MNRAS, 334, 1000

de Vaucouleurs, G., de Vaucouleurs, A., Corwin, J. R., Buta, R. J., Paturel, G., & Fouqué, P., 1991, Third Reference Catalogue of bright galaxies (New York:Springer) (RC3)

Dolphin, A. E., 2000a, WFPC2 Stellar Photometry with HSTPHOT, PASP, 112, 1383

Dolphin, A. E., 2000b, The Charge-Transfer Efficiency and Calibration of WFPC2, PASP, 112, 1387

Dolphin, A. E., & Kennicutt, R. C., 2002a, HUBBLE SPACE TELESCOPE Survey of Clusters in Nearby Galaxies. I. Detection and Photometry, AJ, 123, 207

Dolphin, A. E., & Kennicutt, R. C., 2002b, HUBBLE SPACE TELESCOPE Survey of Clusters in Nearby Galaxies. II. Statistical Analysis of Cluster Populations. AJ. 124. 158

Dolphin, A. E., 2003, HSTphot User's Guide (version 1.1.5b)

Harris, W. E., 1996, A Catalog of Parameters for Globular Clusters in the Milky Way, AJ, 112, 1487

Holtzman, J. A., Burrows, C. J., Casertano, S., Hester, J. J., Trauger, J. T., Watson, A. M., & Worthey, G., 1995, The Photometric Performance and Calibration of WFPC2, PASP, 107, 1065

Jordán, A., Côté, P., West, M. J., Marzke, R. O., & Minniti, D., 2004, Hubble Space Telescope Observations of cD Galaxies and Their Globular Cluster Systems, AJ, 127, 24

Keel, W. C., & Borne, K. D., 2003, Massive Star Clusters in Ongoing Galaxy Interactions: Clues to Cluster Formation, AJ, 126, 1257

Lee, M. G., Chandar, R., & Whitmore, B., 2005, Properties of Resolved Star Clusters in M51, AJ, submitted

Luck, R. E., Moffet, T. J., Barnes, T. G., & Gieren, W. P., 1998, Magellanic Cloud Cepheids - Abundances, AJ, 115, 605

Mackey, A. D, & Gilmore, G. F., 2003, Surface brightness profiles and structural parameters for 53 rich stellar clusters in the Large Magellanic Cloud, MNRAS, 338, 85

Miller, B. W., Whitmore, B. C., Schweizer, F., & Fall, S. M., 1997, The Star Cluster System of the Merger Remnant NGC 7252, AJ, 114, 2381

Sandage, A., R. & Tammann, G., A., 1981, A Revised Shapley-Ames Catalogue (Washington: Carnegie Institution)

Schlegel, D. J., Finkeiner, D. P., & Davis, M., 1998, Maps of Dust Infrared Emission for Use in Estimation of Reddening and Cosmic Microwave Background Radiation Foregrounds, ApJ, 500, 525

Schweizer, F., & Miller, B. W., 1996, Hubble Space Telescope Observations of Candidate Young Globular Clusters and Stellar Associations in the Recent Merger Remnant NGC 3921, AJ, 112, 1839

Seth, A., Olsen, K., Miller, B., Lotz, J., & Telford, R., 2004, Star Clusters in Virgo and Fornax Dwarf Irregular Galaxies, AJ, 127, 789

Whitmore, B. C., 2003, in A Decade of Hubble Space Telescope Proceeding of the Space Telescope Science Institute Symposium, ed. M. Livio, K. Noll & M. Stiavelli (Cambridge, UK: Cambridge University Press), vol. 14, 153, 178

Zepf, S. E., Ashman, k. M., English, J., Freeman, K. C., & Sharples, R. M., 1999, The Formation and Evolution of Candidate Young Globular Clusters in NGC 3256, AJ, 118, 752